

Infinitesimal asphericity changes the universality of the jamming transition

Harukuni Ikeda¹, Carolina Brito², Matthieu Wyart³

¹Laboratoire de Physique de l'Ecole Normale Supérieure, ENS, Université PSL, CNRS, Sorbonne Université, Université de Paris, Paris, France

²Instituto de Física, UFRGS, 91501-970, Porto Alegre, Brazil

³Institute of Physics, EPFL, CH-1015 Lausanne, Switzerland

E-mail: harukuni.ikeda@ens.fr

March 2019

Abstract. The jamming transition of nonspherical particles is fundamentally different from the spherical case. Systems of nonspherical particles are hypostatic at the jamming point, while isostaticity is ensured in the case of the jamming of spherical particles. This structural difference implies that critical exponents related to the contact number and the vibrational density of states are affected in the presence of an asphericity. Moreover, while the force and gap distributions of isostatic jamming present a power-law behavior, even an infinitesimal asphericity is enough to smooth out these singularities. In a recent work [PNAS 115(46), 11736], we have used a combination of marginal stability arguments and the replica method to explain these observations. We argued that systems with internal degrees of freedom, like the rotations in the ellipsoids or spherocylinders or the variation of the radii in the case of the *breathing* particles fall in the same universality class. In this paper we review comprehensively the results about the jamming of nonspherical particles, use theoretical arguments to derive the critical exponents of the contact number, shear modulus, and the characteristic frequencies of the density of states which can be applied for any model having an extra degree of freedom in addition to translational degrees of freedom. Moreover, we present additional numerical data supporting the theoretical results which were not shown in the previous work.

1. Introduction

The jamming of nonspherical particles is qualitatively different from that of spherical particles [2, 3]. Several experimental and numerical investigations uncover that (i) the system of nonspherical particles is not isostatic at the jamming transition point [4], while the system of spherical particles is [5], (ii) the pair correlation of nonspherical particles does not exhibit the power law singularity at the jamming transition point [1], while that of spherical particles does [6], and (iii) the values of critical exponents of nonspherical particles are different from those of spherical particles [7, 8].

The theoretical understanding of the jamming of nonspherical particles is challenging because particles do not hold rotational symmetry. In the previous work [1, 9], we proposed a way to bypass this difficulty by considering the mapping from nonspherical particles to the breathing particles (BP), defined as a system of spherical particles for which their diameters are allowed to fluctuate [10]. An advantage of the BP particles is that the model holds the rotational symmetry, and thus, one can apply the same technique developed for the spherical particle without any difficulty. Using the BP, we theoretically and numerically confirmed that the gap and force distributions of nonspherical particles are regular and finite even at the jamming transition point, while those quantities exhibit the power law in the case of spherical particles. Furthermore, we showed that the critical exponents of several physical quantities such as the contact number, shear modulus, and characteristic frequencies of the density of state have different values from those of spherical particles. This confirms that the jamming of nonspherical particles belongs to the different universality class from that of spherical particles.

This paper is a longer version of our previous work [1]. We shall give a more straight forward derivation of the scaling functions without mapping to the BP particles, and additional numerical data supporting the theoretical results. The organization of the remaining paper is as follows. In Sec. 2, we develop the variational argument for nonspherical particles. In Sec. 3, We discuss the connection between nonspherical particles and BP. In Sec. 4, we discuss the universal form of the gap and force distributions near the isostatic point. In Sec. 5, we discuss the scaling behavior of the density of state of the BP and show that the characteristic frequencies exhibit the same scaling of that of nonspherical particles. In Sec. 6, we summarize and conclude the work.

2. Variational argument for nonspherical particles

Here we derive the scaling functions of nonspherical particles by using the variational argument [11, 12]. In the previous work [1], we performed this calculation by mapping the Gay-Berne potential, which is a model for ellipsoids, to the breathing particles (BP), which is the model consisting of spherical particles where the radii of particles can vary continuously [10]. In this paper, instead, we present a more direct derivation of the scaling functions of nonspherical particles without using the mapping to the BP model.

2.1. Interaction potential

For concreteness, we consider the following interaction potential:

$$V_N = \sum_{i < j} v(h_{ij}), \quad (1)$$

where h_{ij} denotes the minimal distance between the i -th and j -th particles, and $v(h)$ denotes a purely repulsive and finite ranged potential, such as the harmonic potential

$v(h) = h^2\theta(-h)/2$, where $\theta(x)$ denotes the Heaviside function.

2.2. Perturbation around a spherical particle

For nonspherical particle, a particle has the rotational degree of freedom in addition to the positional degree of freedom. We assign the vectors \mathbf{x}_i and a unit vector \mathbf{u}_i to express the position and direction of the i -th particle, respectively. The radius σ_i of a nonspherical particles along direction \hat{r} varies depending on both \mathbf{u}_i and \hat{r} . We shall assume that there is a small parameter Δ representing the deviation from the spherical particles. We expand the diameter using Δ as

$$\sigma_i(\hat{r}, \mathbf{u}_i) = \sigma^{(0)} + f(\hat{r}, \mathbf{u}_i)\Delta + O(\Delta^2), \quad (2)$$

where $\sigma^{(0)}$ represents the diameter of the reference sphere, and $f(\hat{r}, \mathbf{u})$ represents the coefficient of the first order term. Following the similar procedure, one can expand the gap function, which is the minimal distance between the i -th and j -th particles. The first order correction of Δ comes from the change of radius of the i -th and j -th particles along the direction $\hat{r}_{ij} = (\mathbf{x}_i - \mathbf{x}_j)/|\mathbf{x}_i - \mathbf{x}_j|$, namely,

$$h_{ij}(\Delta) - h_{ij}^{(0)} = -\Delta [f(\hat{r}_{ij}, \mathbf{u}_i) + f(-\hat{r}_{ij}, \mathbf{u}_j)] + O(\Delta^2), \quad (3)$$

where $h_{ij}^{(0)}$ denotes the gap function of the reference spherical particles:

$$h_{ij}^{(0)} \equiv h_{ij}(0) = r_{ij} - \sigma_i^{(0)} - \sigma_j^{(0)}. \quad (4)$$

Substituting this into eq. (1) and expanding by Δ , we have

$$V_N = U_N + \mu_N, \quad (5)$$

where

$$\begin{aligned} U_N &= \sum_{i < j} \left[v(h_{ij}^{(0)}) + w_{ij}\Delta^2 \right], \\ \mu_N &= \sum_i g_i(\mathbf{u}_i). \end{aligned} \quad (6)$$

Here $w_{ij}\Delta^2$ denotes the $O(\Delta^2)$ terms of the interaction potential, and we have introduced the auxiliary function as

$$g_i(\mathbf{u}_i) = -\Delta \sum_{j \neq i} v'(h_{ij}^{(0)}) [f'(\hat{r}_{ij}, \mathbf{u}_i) + f'(-\hat{r}_{ij}, \mathbf{u}_i)]. \quad (7)$$

From eqs. (6) and (7), one can show that

$$\mu_N \sim g_i \sim p\Delta, \quad (8)$$

where $p \sim v'(h)$ denotes the pressure.

To clarify the physical meaning of Δ , it is convenient to clarify the relation between Δ and the sphericity \mathcal{A} , which represents how far is the shape of a particle from a perfect sphere; $\mathcal{A} = 1$ for the perfect sphere and $\mathcal{A} > 1$ otherwise. Since \mathcal{A} takes a minimal value at $\Delta = 0$, one can expand it as $\mathcal{A}(\Delta) = 1 + \frac{1}{2}\mathcal{A}''(0)\Delta^2 + O(\Delta^3)$, implying that

$$\Delta \sim (\mathcal{A} - 1)^{1/2}. \quad (9)$$

This is a useful relation to compare with the numerical and experimental results.

2.3. Variational argument

Near the jamming transition point $p \ll 1$, the constraints can be classified into “hard” and “soft”: the energy cost to violate a hard constraint remains finite at $p = 0$, while that of the soft constraint is $O(p)$. At $p = 0$, μ_N vanishes and U_N gives the hard constants. The number of hard constraints is

$$N_c^{\text{hard}} = \frac{Nz}{2}, \quad (10)$$

where N denotes the number of particles, and z denotes the contact number per particle. Then, the number of unconstrained modes, which we hereafter refer to as the *zero modes*, is

$$N_0 = N(d + d_{\text{rot}}) - N_c^{\text{hard}} = Nd_{\text{rot}} - \frac{N}{2}\delta z, \quad (11)$$

where $\delta z = z - 2d$, and d_{rot} denotes the number of degree of freedom of rotation per particle. For $p > 0$, μ_N has a finite value which would stabilize some of the zero modes. μ_N gives $N_c^{\text{soft}} = Nd_{\text{rot}}$ number of soft constraints, the typical stiffness of which is $k_R = \partial_{\mathbf{u}_i} \partial_{\mathbf{u}_j} \mu_N \sim p\Delta$. The number of soft modes is indeed suffice to stabilize the zero modes:

$$N_c^{\text{soft}} - N_0 = \frac{N}{2}\delta z > 0. \quad (12)$$

If $\delta z \ll 1$, the system is nearly isostatic and the minimal eigenvalue of the zero mode is calculated by applying the standard variational argument of the jamming of spherical particles [12]. Using the variational argument, one can show that the order $O(\Delta)$ term of the minimal eigenvalue proportional to $k_R \delta z^2 \sim p\Delta \delta z^2$. Up to order $O(\Delta^2)$, the minimal eigenvalue of the zero modes can be written as

$$\lambda_{\min} = p [c_1 \Delta \delta z^2 + c_2 \Delta^2 + O(\Delta^3)], \quad (13)$$

where all terms should be proportional to p , because the zero mode vanishes as p . The marginal stability requires $\lambda_{\min} = 0$, meaning that the first and second terms in eq. (13) should be canceled each other, which leads to the scaling of δz :

$$\delta z \sim \Delta^{1/2} \sim (\mathcal{A} - 1)^{1/4}. \quad (14)$$

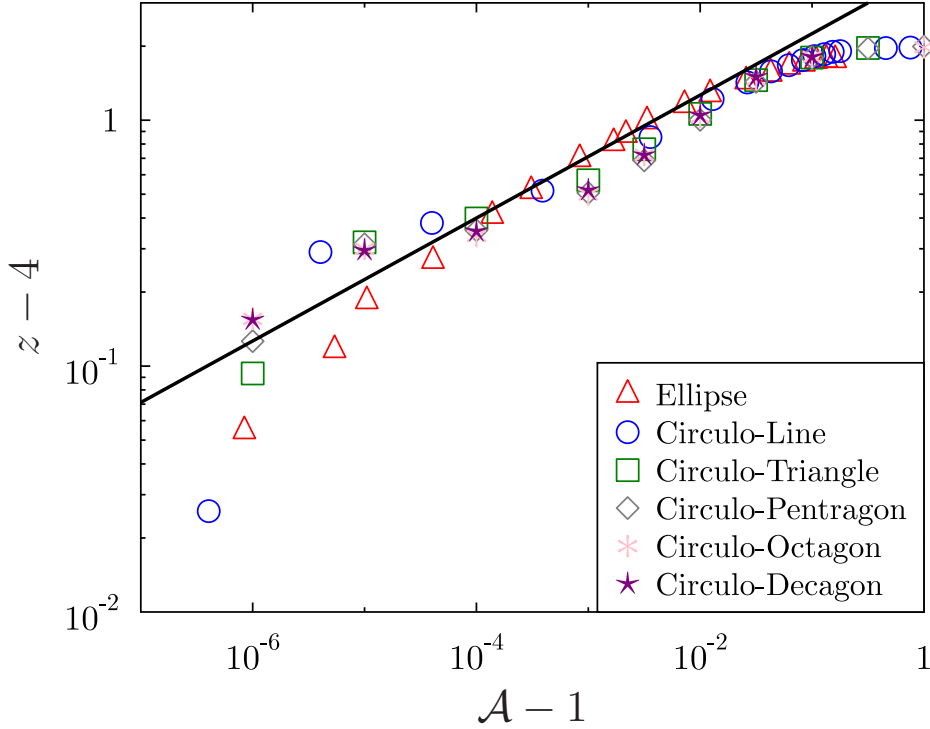


Figure 1. Scaling of the contact number of nonspherical particles. The symbols denote the numerical results, and the solid line denotes the theoretical prediction $z - 4 \sim (\mathcal{A} - 1)^{1/4}$. Data for nonspherical particles are taken from Ref. [13].

In Fig. 1, we compare the theoretical prediction, eq. (14), with the numerical results of various shapes of nonspherical particles. We get the excellent agreement with the theory and numerical result, though there are visible deviations for $\mathcal{A} - 1 \ll 1$, which might be originated from the lack of statistics or numerical precision.

In the $\Delta \rightarrow 0$ limit, Eq. (14) should be smoothly connected to the result of spherical particles [12]:

$$\delta z \sim p^{1/2}. \quad (15)$$

From eqs. (14) and (15), one can decide the scaling form of δz as

$$\delta z = \Delta^{1/2} \mathcal{Z}(\Delta^{-1}p), \quad (16)$$

where

$$\mathcal{Z}(x) = \begin{cases} \text{const} & (x \ll 1), \\ x^{1/2} & (x \gg 1). \end{cases} \quad (17)$$

$\mathcal{Z}(x)$ is a finite and regular function at $x = 0$, and thus one can expand it as $\mathcal{Z}(x) = \mathcal{Z}(0) + \mathcal{Z}'(0)x + \dots$, which leads to

$$z - z_J \sim \frac{p}{\Delta^{1/2}}, \quad (18)$$

where $z_J = 2d + \Delta^{1/2}\mathcal{Z}(0)$. This is again consistent with the numerical result of ellipsoids [14]. We now turn our attention to the scaling of the shear modulus G . In the standard numerical procedure to calculate G , one first imposes the small strain and then minimizes the energy. Comparing the resultant energy with that of the undeformed one, one can calculate G [15]. Previous numerical and theoretical investigations prove that the square root singularity $G \sim p^{1/2}$ appears near the jamming transition of spherical particles [15, 11]. We here discuss how this scaling is altered for nonspherical particles. We assume that the imposed shear excites only the zero modes because the typical energy of those modes is much smaller than the other near the jamming transition point. When $\Delta \ll 1$, the zero modes mainly consists of the rotational degree of freedom and thus $\delta u_i \sim \delta\gamma/\Delta$, where $\delta\gamma$ denotes the imposed shear strain, and δu_i denotes the displacement caused by the imposed shear. This increases the energy as

$$\delta V_N \sim \delta\mu_N \sim \min_{\mathbf{y}_i} \sum_{i=1}^N \sum_{\alpha=1}^{d_{\text{rot}}} k_i^\alpha (\delta \tilde{u}_i^\alpha + y_i^\alpha)^2, \quad (19)$$

where k_i and $\tilde{\mathbf{u}}_i$ denotes the eigenvalue and eigenvector of $\partial_{\mathbf{u}_i^\alpha} \partial_{\mathbf{u}_i^\beta} g_i(\mathbf{u}_i)$, and \mathbf{y}_i denotes the vector spanned by the N_0 zero modes. Using the standard technique of the linear algebra, one can eliminate N_0 terms among Nd_{rot} terms in eq. (19) (see. Ch.7 in Ref. [16]). Thus, the typical amplitude of δV_N is

$$\delta V_N \sim k_R(Nd_{\text{rot}} - N_0) \left(\frac{\delta\gamma}{\Delta} \right)^2 \sim \frac{Np\delta z\delta\gamma^2}{\Delta}. \quad (20)$$

The shear modulus G is then calculated as

$$G \sim \frac{\delta V_N}{N\delta\gamma^2} \sim \frac{p}{\Delta^{1/2}}. \quad (21)$$

The result is consistent with the numerical results of ellipsoids [7]. In the $\Delta \rightarrow 0$ limit, Eq. (21) smoothly connects to the result of spherical particles [15, 11],

$$G \sim p^{1/2}. \quad (22)$$

This requires the following scaling form:

$$G = \Delta^{1/2}\mathcal{G}(\Delta^{-1}p), \quad (23)$$

where the scaling function $\mathcal{G}(x)$ satisfies

$$\mathcal{G}(x) = \begin{cases} x & (x \ll 1), \\ x^{1/2} & (x \gg 1). \end{cases} \quad (24)$$

In Fig. 2, we confirm our scaling prediction for ellipsoids interacting with harmonic potential, where Δ can be identified with the aspect ratio. For the harmonic potential, the pressure is proportional to the distance to the jamming transition point, which allows us to replace p in eq. (23) by $\delta\varphi = \varphi_J - \varphi$. One can see that the data of different aspect ratios are collapsed on a single curve, proving the validity of the scaling prediction eq. (23).

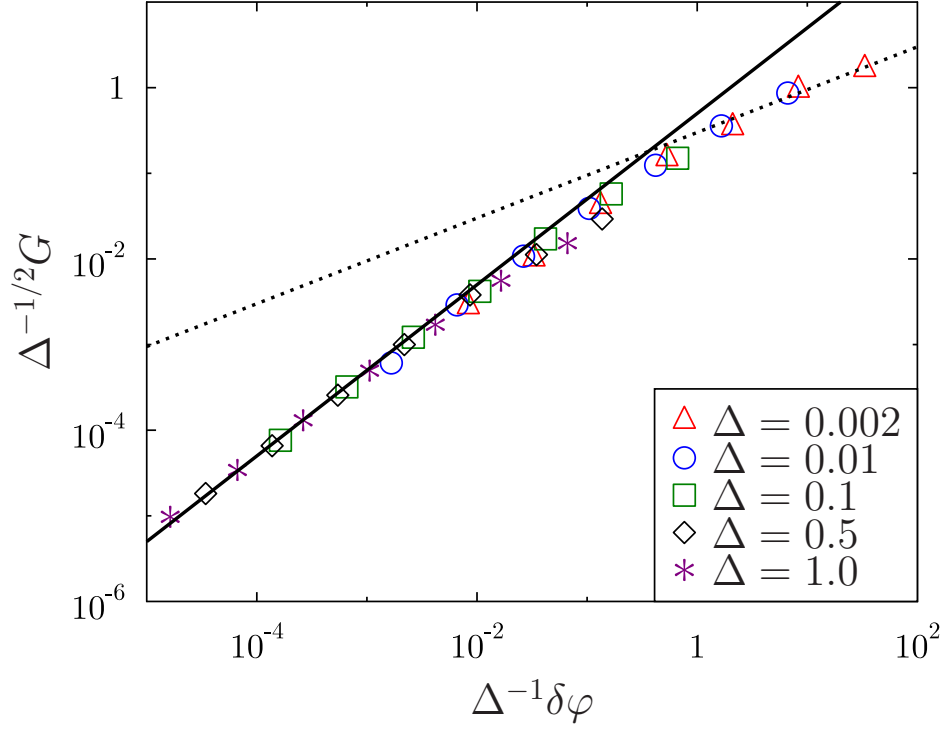


Figure 2. Saling plot of the shear modulus of ellipsoids. The symbols denote the numerical results. The solid and dotted lines denote the theoretical predictions $G \sim \delta\varphi$ and $G \sim \delta\varphi^{1/2}$, respectively. Data are taken from Ref. [7].

3. Connection between nonspherical particles and breathing particles

The above argument can be generally applied for the models having extra degrees of freedoms, in addition to the translational degrees of freedom. Besides nonspherical particles, another interesting model which belongs to the same universality class is the so-called breathing particle (BP) model [1]. The model consists of N polydisperse particles whose radius will evolve with time. The interaction potential of the model is given by

$$V_N = U_N + \mu_N, \quad (25)$$

where

$$U_N = \sum_{i < j} \frac{h_{ij}^2}{2} \theta(-h_{ij}), \quad h_{ij} = r_{ij} - R_i - R_j, \quad (26)$$

and

$$\mu_N = \frac{k}{2} \sum_i (R_i - R_i^0)^2 \left(\frac{R_i^0}{R_i} \right)^2. \quad (27)$$

The stiffness k of the chemical potential is chosen so to fix the variance of the diameter:

$$\Delta \propto \sqrt{\frac{1}{NR_0^2} \sum_i (R_i - R_i^0)^2}. \quad (28)$$

From the saddle point condition, $\partial_{R_i} V_N = 0$, one can infer that

$$k \sim \frac{p}{\Delta}. \quad (29)$$

By introducing the new variable $u_i \equiv (R_i - R_i^0)/\Delta$, eqs. (26) and (27) can be rewritten as

$$\begin{aligned} U_N &= \sum_{i<j} \frac{h_{ij}^2}{2} \theta(-h_{ij}), & h_{ij} &= r_{ij} - R_i^0 - R_j^0 + \Delta(u_i + u_j), \\ \mu_N &= \frac{k_R}{2} \sum_i u_i^2 \left(\frac{R_i^0}{R_i^0 + \Delta u_i} \right)^2, \end{aligned} \quad (30)$$

where

$$k_R = \Delta^2 k \sim \Delta p. \quad (31)$$

Note that the stiffness of the chemical potential k_R now has the same order as that of nonspherical particles. Thus, one can repeat the same argument in the previous sections for nonspherical particles, which leads to the same critical exponents [1]. The numerical implementation of the BP model is rather simpler and the calculation time is shorter than those of nonspherical particles, as the extra degree of freedom is a simple scalar variable. For this reason, we shall use the BP in the numerical experiments in the following sections, instead of nonspherical particles. To obtain jammed configurations of the BP system, use the FIRE algorithm to find the inherent structures of the potential Eq.(30). We use the Barendsen barostat to find them at fixed pressure. All the details are explained in the [1]. Most of the results shown in the following are made for a system with $N = 484$ particles. When this is not the case, it is explicitly written.

4. Universal scaling of the gap and force distributions near isostatic point

Here we show that the gap and force distributions exhibit the universal scaling behavior near the isostatic point.

4.1. Definition of the distribution functions

Here we investigate the gap distribution

$$\rho(h) \equiv \frac{1}{N} \left\langle \sum_{i<j} \delta(h_{ij} - h) \right\rangle. \quad (32)$$

At the zero temperature $T = 0$, $\rho(h)$ has the gap at $h = 0$ [15]. For this reason, it is convenient to define the distributions for the positive and negative h , separately. We define the positive gap distribution

$$g(h) \equiv \theta(h) \frac{\rho(h)}{\int_0^\infty dh \rho(h)}, \quad (33)$$

and the force (normalized negative gap) distribution

$$P(f) \equiv \theta(-h) \frac{\rho(h) \frac{dh}{df}}{\int_{-\infty}^0 \rho(h) \frac{dh}{df} df}, \quad (34)$$

where $\theta(x)$ is the Heviside function, and $f = -h/p$. It is well known that at the jamming transition point of spherical particles, $g(h)$ and $P(f)$ exhibit the power law for small h and f [6, 17]:

$$\begin{aligned} g(h) &\sim h^{-\gamma}, \\ P(f) &\sim f^\theta. \end{aligned} \quad (35)$$

Below, we discuss that the power law is generally truncated at finite h and f if the system is not isostatic.

4.2. Finite size scaling

Here we first describe the distribution functions of finite N system. Then, in the next subsection, we show that the scaling of finite N can be generalized to the scaling of non-isostatic system.

The minimal gap h_{\min} of the N particle system is calculated by using the extreme statistics [18]

$$\int_0^{h_{\min}} g(h) dh \sim h_{\min}^{1-\gamma} \sim \frac{1}{N} \Rightarrow h_{\min} \sim N^{-\frac{1}{1-\gamma}}. \quad (36)$$

When $h \ll h_{\min}$, $g(h)$ quickly decreases, implying that the power law divergence of $g(h)$, eq. (35), is truncated at $h \sim h_{\min}$. $g(h)$ is regular and finite for $h \ll h_{\min}$. Thus, the scaling form of $g(h)$ at finite N would be [18]

$$g(h) \sim \begin{cases} N^{\mu\gamma} p_0^+(hN^\mu) & (h \sim N^{-\mu}), \\ h^{-\gamma} & (h \sim 1) \end{cases}, \quad (37)$$

where $p_0^+(x)$ is a regular and finite function and

$$\mu = \frac{1}{1-\gamma}. \quad (38)$$

We perform the numerical simulation for two dimensional harmonic spheres to test

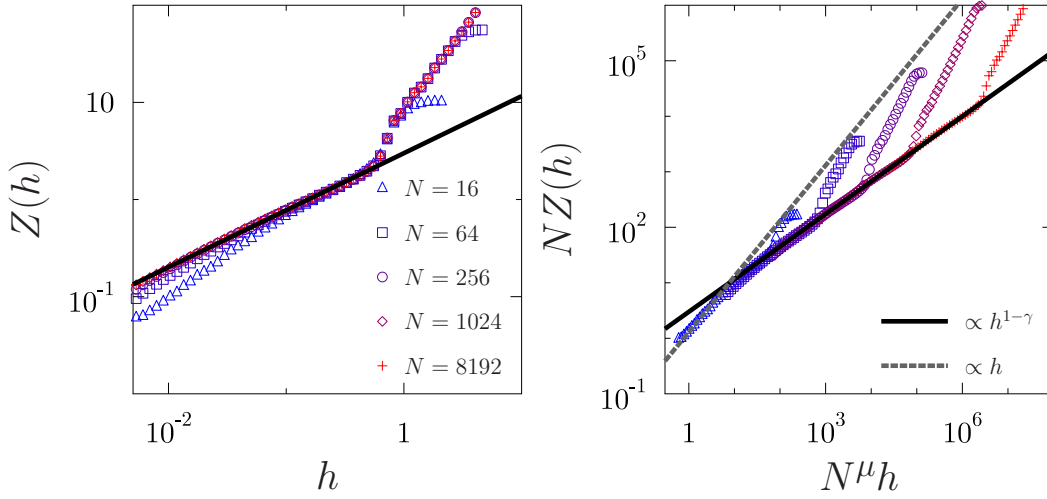


Figure 3. Cumulative gap distribution (left) and its scaling plot (right). Symbols are results of numerical simulations of the harmonic potential at the jamming point for different system sizes and the lines are theoretical predictions.

the above conjecture. Instead of $g(h)$, we observe the cumulative distribution $Z(h) = \int_0^h dh' g(h')$ to improve the statistics. From eq. (37), $Z(h)$ should satisfy

$$Z(h) \sim \begin{cases} N p_0^+(h N^\mu) & (h \sim N^{-\mu}), \\ h^{1-\gamma} & (h \sim 1) \end{cases}. \quad (39)$$

In Fig. 3, we plot $Z(h)$ and its scaling form for various N , which exhibits an excellent scaling collapse.

4.3. General scaling form of the distribution functions near isostatic point

We want to generalize the above argument for more general systems close to the isostatic point, namely, $\delta z \ll 1$. For this purpose, we shall consider some function $F(h)$ which has the following scaling form for $\delta z \ll 1$:

$$F(h) = \delta z^\alpha \mathcal{F}(\delta z^\beta h), \quad (40)$$

where α and β denote the critical exponents we want to determine from the finite size scaling. The extensive numerical simulations of spherical particles of the various system sizes prove that the scaling like eq. (40) persists up to $\delta z = 1/N$ [19, 20], suggesting that for the finite size system at the jamming transition point, we have

$$F(h) = N^{-\alpha} \mathcal{F}(N^{-\beta} h). \quad (41)$$

In other words, the scaling for $\delta z \ll 1$ can be obtained by substituting $N = \delta z^{-1}$ into the result of the finite size scaling. From eqs. (37) and (39), we have

$$g(h) \sim \begin{cases} \delta z^{-\mu\gamma} p_0^+(h \delta z^{-\mu}) & (h \sim \delta z^\mu) \\ h^{-\gamma} & (h \sim 1) \end{cases}, \quad (42)$$

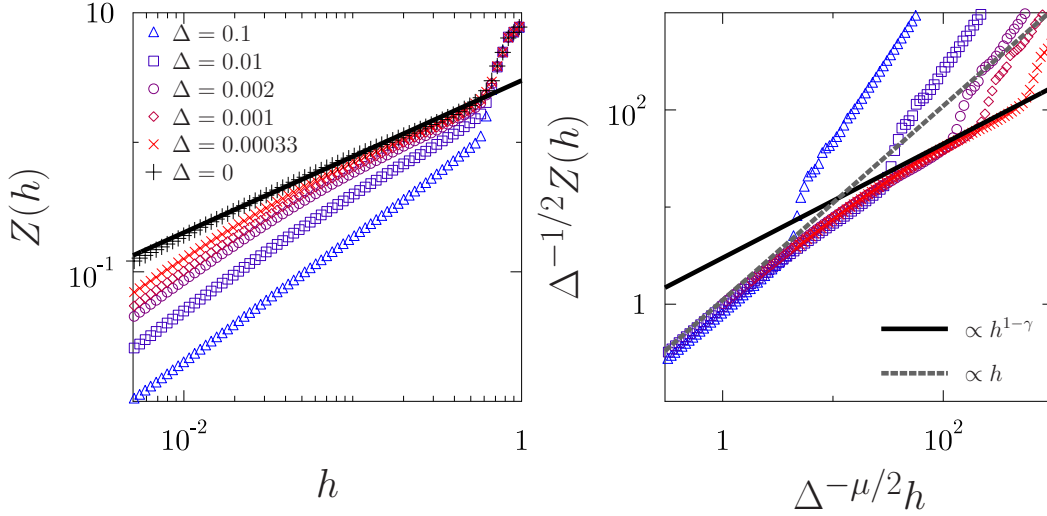


Figure 4. Cumulative gap distribution (left) of nonspherical particles and its scaling plot (right). Symbols are results of numerical simulations of the BP system for different values of variance of the diameter Δ and a system with $N=8192$ particles. Lines are theoretical predictions.

and

$$Z(h) \sim \begin{cases} \delta z^{-1} p_0^+(h \delta z^{-\mu}) & (h \sim \delta z^\mu) \\ h^{1-\gamma} & (h \sim 1) \end{cases}. \quad (43)$$

We propose that the above equations hold for any system sufficiently near the isostatic point, *i.e.*, $\delta z \ll 1$. We shall test this conjecture for the BP at the jamming transition point, at which we have shown that $\delta z \sim \Delta^{1/2}$ [1]. In Fig. 4, we show $Z(h)$ and its scaling form of the BP at the jamming transition point. The excellent scaling collapse justifies the validity of eqs. (42) and (43). Note that the same equation of eq. (42) holds exactly in the case of mean-field model of nonspherical particles [1, 9] and the spherical particles slightly above the jamming transition point, where $\delta z \sim p^{1/2}$ [21].

For the force distribution $P(f)$, one can apply a similar argument, and it has been shown that

$$P(f) \sim \begin{cases} \delta z^{\theta\nu} p_0^-(f \delta z^{-\nu}) & (f \sim \delta z^\nu) \\ f^\theta & (f \sim 1) \end{cases}, \quad (44)$$

where $p_0^-(x)$ denotes a finite and regular function, and we have introduced the critical exponents by

$$\nu = \frac{1}{1 + \theta}. \quad (45)$$

The numerical justification of $P(f)$ is rather tricky because one should carefully separate the localized and extended modes to compare with the theoretical prediction [22], which we leave for future work.

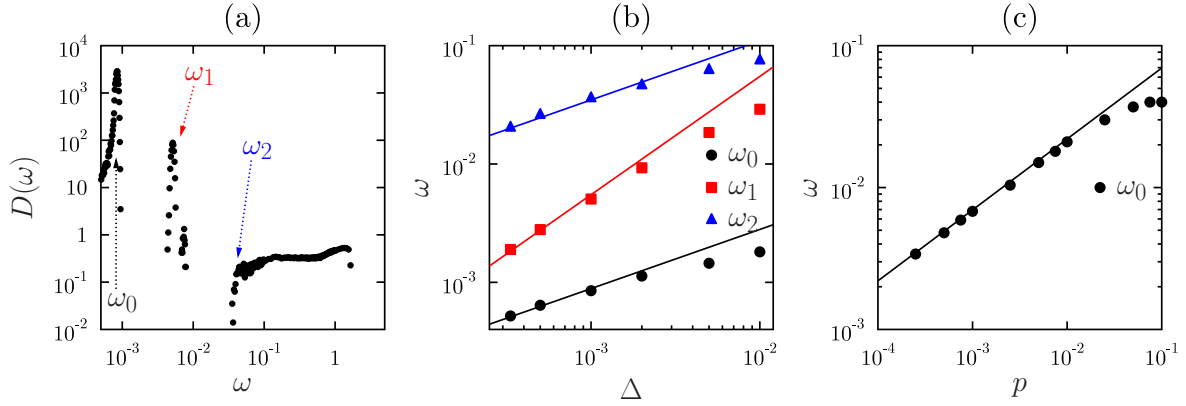


Figure 5. (a) Density of states $D(\omega)$ for the BP system at $\Delta = 10^{-3}$ and $p = 10^{-4}$ and the definition of the characteristic frequencies. (b) The Δ dependence of the characteristic frequencies. Lines are theoretical predictions, $\omega_0 \propto \Delta^{1/2}$, $\omega_1 \propto \Delta$, and $\omega_2 \propto \Delta^{1/2}$ (c) The p dependence of the characteristic frequencies. Line is the theoretical prediction, $\omega_0 \propto p^{1/2}$.

5. Vibrational density of state

The vibrational density of state $D(\omega)$ plays the central role to characterize the low temperature physics of solids [23]. In this section, we investigate $D(\omega)$ of the BP model near the jamming transition point, which exhibits the same scaling of that of nonspherical particles.

5.1. Characteristic frequencies

We first describe the qualitative shape of $D(\omega)$ and define the characteristic frequencies. In Fig. 5 (a), we show the typical behavior of $D(\omega)$ of the BP model. $D(\omega)$ consists of the three separate parts: (i) the lowest band at ω_0 , (ii) the intermediate band at ω_1 , and (iii) the highest band starts from ω_2 . In Fig 5 (b), we show the Δ dependence of the characteristic frequencies, ω_0 , ω_1 , and ω_2 . The characteristic frequencies are well fitted by the following power laws (see solid lines):

$$\omega_0 \sim \Delta^{1/2}, \quad \omega_1 \sim \Delta, \quad \omega_2 \sim \Delta^{1/2}. \quad (46)$$

In Fig. 5 (c), we show the p dependence of ω_0 . We found that

$$\omega_0 \sim p^{1/2}, \quad (47)$$

while ω_1 and ω_2 remain constant (not shown). The above scaling is the same of that of ellipsoids if we identify Δ with the aspect ratio [8], which is another evidence that the BP and ellipsoids belong to the same universality class.

Using the previous theoretical analysis [1, 9], one can interpret the above results as follows: (i) The lowest band corresponds to the zero modes stabilized by the positive part of the pre-stress. As the pre-stress scales as $k_R \sim p\Delta$, eq. (31), the characteristic

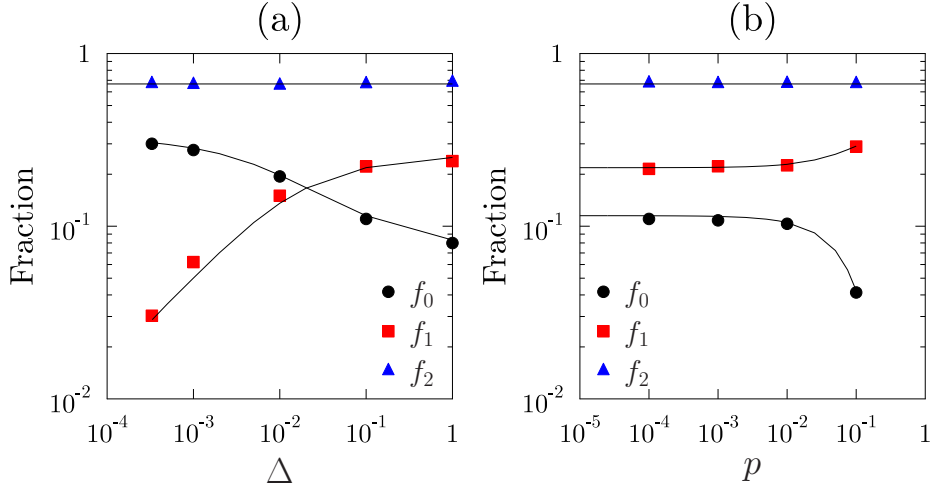


Figure 6. The weights of the three bands of the $D(\omega)$ as the example shown in Fig.(5)-a. Symbols are numerical results for the BP system as function of p at fixed $\Delta = 10^{-1}$ (a) and as a function of Δ at fixed pressure $p = 10^4$ (b). Solid lines are the theoretical predictions, see the main text.

frequency of the mode is $\omega_0 \sim \sqrt{k_R} \sim p^{1/2} \Delta^{1/2}$. (ii) the intermediate band corresponds to the breathing motion of the BP or the rotation of ellipsoids. The characteristic frequency is $\omega_1 \sim \sqrt{\partial_R^2 V_N} \sim \Delta$. (iii) the highest band corresponds to the translational degree of freedom. As in the case of spherical particles, the characteristic frequency is proportional to δz [16]. Using eq. (14), we get $\omega_2 \sim \Delta^{1/2}$. Herewith we recover the above numerical results. To give further evidence to support the above picture, we calculate the weights of each band by numerically integrating $D(\omega)$. If the above description is correct, one should have the following equations:

$$N_0 = N \left(1 - \frac{\delta z}{2} \right), \quad N_1 = \frac{N \delta z}{2}, \quad N_2 = dN, \quad (48)$$

where N_i denotes the number of the modes included in the i -th band. Since the total number of modes is $3N$, the fraction f_i of modes in each band is given by $f_i = N_i/3N$. In Fig. 6, we show the Δ and p dependence of f_i and compare with the theoretical prediction eqs. (48). We obtain quite good agreement.

6. Summary and discussions

In this paper, we investigated the jamming transition of nonspherical particles and breathing particles. Using both numerical and scaling argument, we confirmed that the critical behavior of the jamming of nonspherical particles and breathing particles is qualitatively different from that of spherical particles. In the left panel of Fig. 7, we summarize our scaling prediction for the shear modulus G . Note that, for non-spherical particles ($\Delta > 0$), G always shows the linear pressure p dependence sufficiently near the jamming transition point ($p \ll 1$), while it exhibits the square root dependence

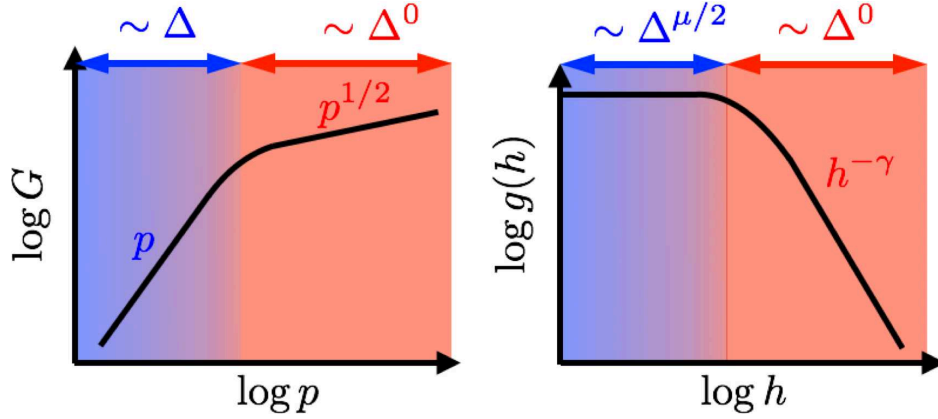


Figure 7. Summary of the scaling prediction. Δ denotes the linear deviation from the spherical particles. (left) The shear modulus G as a function of the pressure p . G exhibits the linear p dependence near jamming $p \ll \Delta$, which it exhibits the square root dependence far from jamming $p \gg \Delta$. (right) The gap distribution $g(h)$. $g(h)$ exhibits the power law $g(h) \sim h^{-\gamma}$ for $h \gg \Delta^{\mu/2}$, while it converges to a finite value for $h \ll \Delta^{\mu/2}$.

for spherical particles ($\Delta = 0$). This means that the critical exponent of G changes discontinuously at $\Delta = 0$ from one to one half, in other word, the small asphericity is enough to change the universality class of the jamming transition. We also show that nonspherical particles and breathing particles are not critical at the jamming transition point in terms of the gap distribution $g(h)$, see the right panel of Fig. 7. The power law divergence of $g(h)$, observed in the case of spherical particles, is truncated at finite h , and thus the gap distribution is finite and analytic even at the jamming transition point. This is a sharp contrast to spherical particles, where the power law divergence of $g(h)$ persists up to $h = 0$. Furthermore, we fully characterized the scaling of the characteristic frequencies of the density of states near the jamming transition point, which are again dramatically different from those of spherical particles.

There are still several open questions. A tentative list is the following:

- From a practical point of view, it is important to understand the rheological properties of the system near the jamming transition point. It has been shown that the divergence of the viscosity is strongly connected to the lowest excitation of the density of state [24]. As discussed in Sec. 5, the density of states of nonspherical particles is very different from that of spherical particles, which would change the critical exponent of the viscosity compared to that of spherical particles. A further study of this point is left as an open problem.
- In this work, we assumed that the two particles could have at most one contact. This assumption is correct for particles of convex shape. However, for particles of non-convex shape, the two particles can have more than two contacts. The extension of our work for such non-convex shape particles is an interesting future work. We believe that the study along this direction would be a promising way to

introduce the effect of the friction, which is considered to be originated from the surface roughness of the constituent particles.

Acknowledgments

We thank F. Zamponi and P. Urbani for previous joint research [1] on which this work is based.

This project has received funding from the European Research Council (ERC) under the European Union’s Horizon 2020 research and innovation programme (grant agreement n.723955-GlassUniversality). This work was supported by a grant from the Simons Foundation (#454953, Matthieu Wyart and #454955).

References

- [1] Brito C, Ikeda H, Urbani P, Wyart M and Zamponi F 2018 *Proceedings of the National Academy of Sciences* **115** 11736–11741
- [2] Van Hecke M 2009 *Journal of Physics: Condensed Matter* **22** 033101
- [3] Torquato S and Stillinger F H 2010 *Rev. Mod. Phys.* **82**(3) 2633–2672 URL <https://link.aps.org/doi/10.1103/RevModPhys.82.2633>
- [4] Donev A, Cisse I, Sachs D, Variano E A, Stillinger F H, Connelly R, Torquato S and Chaikin P M 2004 *Science* **303** 990–993
- [5] Bernal J and Mason J 1960 *Nature* **188** 910
- [6] Donev A, Torquato S and Stillinger F H 2005 *Phys. Rev. E* **71**(1) 011105 URL <https://link.aps.org/doi/10.1103/PhysRevE.71.011105>
- [7] Mailman M, Schreck C F, O’Hern C S and Chakraborty B 2009 *Phys. Rev. Lett.* **102**(25) 255501 URL <https://link.aps.org/doi/10.1103/PhysRevLett.102.255501>
- [8] Schreck C F, Mailman M, Chakraborty B and O’Hern C S 2012 *Phys. Rev. E* **85**(6) 061305 URL <https://link.aps.org/doi/10.1103/PhysRevE.85.061305>
- [9] Ikeda H, Urbani P and Zamponi F 2019 *Journal of Physics A: Mathematical and Theoretical* **52** 344001
- [10] Brito C, Lerner E and Wyart M 2018 *Phys. Rev. X* **8**(3) 031050 URL <https://link.aps.org/doi/10.1103/PhysRevX.8.031050>
- [11] Wyart M, Silbert L E, Nagel S R and Witten T A 2005 *Phys. Rev. E* **72**(5) 051306 URL <https://link.aps.org/doi/10.1103/PhysRevE.72.051306>
- [12] Yan L, DeGiuli E and Wyart M 2016 *EPL (Europhysics Letters)* **114** 26003
- [13] VanderWerf K, Jin W, Shattuck M D and O’Hern C S 2018 *Phys. Rev. E* **97**(1) 012909 URL <https://link.aps.org/doi/10.1103/PhysRevE.97.012909>
- [14] Schreck C F, Xu N and O’Hern C S 2010 *Soft Matter* **6** 2960–2969
- [15] O’Hern C S, Silbert L E, Liu A J and Nagel S R 2003 *Phys. Rev. E* **68**(1) 011306 URL <https://link.aps.org/doi/10.1103/PhysRevE.68.011306>
- [16] Wyart M 2005 *arXiv preprint cond-mat/0512155*
- [17] Charbonneau P, Corwin E I, Parisi G and Zamponi F 2012 *Phys. Rev. Lett.* **109**(20) 205501 URL <https://link.aps.org/doi/10.1103/PhysRevLett.109.205501>
- [18] Kallus Y 2016 *Phys. Rev. E* **93**(1) 012902 URL <https://link.aps.org/doi/10.1103/PhysRevE.93.012902>
- [19] Goodrich C P, Liu A J and Nagel S R 2012 *Phys. Rev. Lett.* **109**(9) 095704 URL <https://link.aps.org/doi/10.1103/PhysRevLett.109.095704>
- [20] Goodrich C P, Liu A J and Sethna J P 2016 *Proceedings of the National Academy of Sciences* **113** 9745–9750

- [21] Franz S, Parisi G, Sevelev M, Urbani P and Zamponi F 2017 *SciPost Phys.* **2**(3) 019 URL <https://scipost.org/10.21468/SciPostPhys.2.3.019>
- [22] Charbonneau P, Corwin E I, Parisi G and Zamponi F 2015 *Phys. Rev. Lett.* **114**(12) 125504 URL <https://link.aps.org/doi/10.1103/PhysRevLett.114.125504>
- [23] Kittel C, McEuen P and McEuen P 1996 *Introduction to solid state physics* vol 8 (Wiley New York)
- [24] Lerner E, Düring G and Wyart M 2012 *Proceedings of the National Academy of Sciences* **109** 4798–4803